CHAPTER 4

Structural Investigation of Fe_3O_4 and $Ag@Fe_3O_4$ Core-Shell Nanoparticles

4.1 Introduction

In the previous chapter, a theoretical investigation for the silver coated magnetite nanoparticles with distinct core sizes and shell thickness have been discussed to obtain the appropriate size range for desired applications. The magnetite and silver coated magnetite nanoparticles with overall size smaller than 40 nm have been synthesized after the optimization of the synthesis parameters. This size has been taken into account after the theoretical simulations carried out in the previous chapter to find the critical size range for a nanoparticle system to behave as a multimodal imaging agent. It turned out that the core-size around 6 nm with varying shell thickness is the most suitable size for obtaining a SPR emission in the blue-green region. The magnetite nanoparticles of average size ~6 and ~8 nm have been synthesized and further coated with silver shell of varying thickness using the optimized parameters of microemulsion synthesis method describe in chapter 2 section 2.7. The structural and composition of the samples have then been

carried out using XRD, TEM and EDAX. The monodispersity of the samples have been confirmed using DLS method as explained in the following sections.

4.2 Structural Characterization of Uncoated and Silver Coated Magnetite Core-Shell Nanoparticles

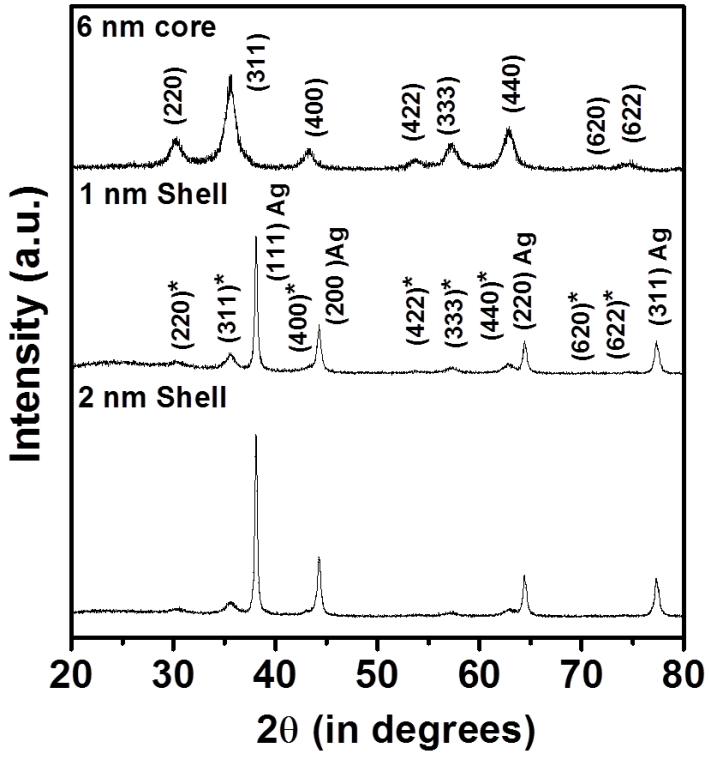

Figure 4.1 XRD pattern of uncoated and silver coated nanoparticles with shell thickness < 2 nm and ~2 nm. *marked peaks in XRD pattern of coated nanoparticles correspond to the magnetite nanoparticles.

Figures 4.1 and 4.2 show X-ray diffraction patterns for uncoated and silver coated magnetite nanostructures with different shell thickness. The analysis confirmed formation of pure phase cubic spinel structured magnetite nanoparticles (space group $Fd\bar{3}m$, 227) and presence of silver (space group $Fm\bar{3}m$, 225) in coated magnetite nanoparticles. The wider peaks in X-ray diffraction spectrum revealed the formation of nanoparticles.

The crystallite size of pure phase magnetite nanoparticles is found to be 6.3 ±0.4 nm nm, calculated using Scherrer formula [162]: $d_{cry}= \frac{0.9\lambda}{\beta\ cos\theta}$; where λ, β and θ are wavelength of incident CuKα radiation, FWHM and Bragg's angle. In silver coated magnetite nanoparticles, the characteristic peaks of both silver and magnetite are observable with relatively less intense magnetite peaks indicating silver coating over magnetite core.

Figures 4.3 and 4.4 represents the bright field TEM images for uncoated and coated

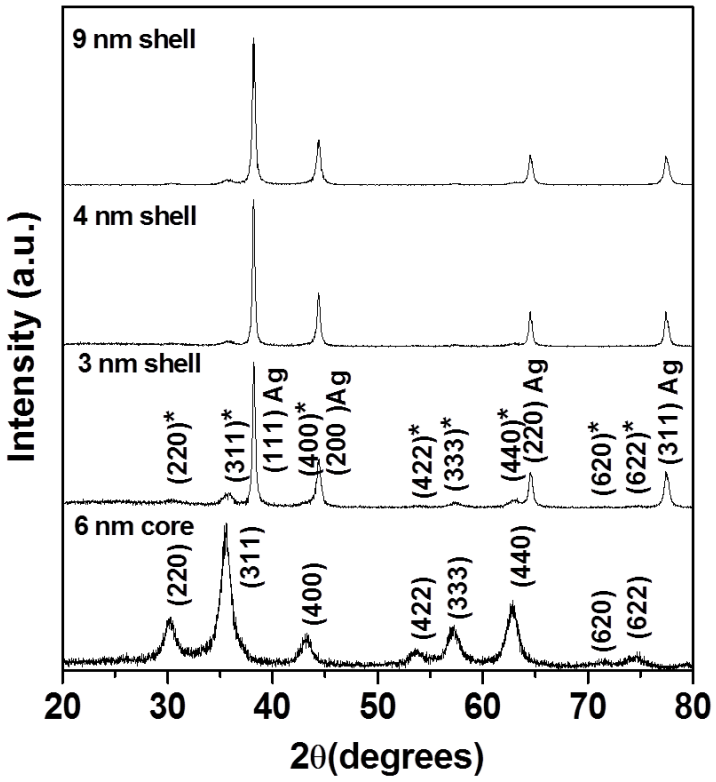

Figure 4.2 XRD pattern of uncoated and silver coated nanoparticles with shell thickness ~3, ~4 and ~9 nm. *marked peaks in XRD pattern of coated nanoparticles correspond to the magnetite nanoparticles.

nanoparticles to measure the particle size and its distribution. The image clearly shows particles of nanometer range with narrower size distribution. The particle size distribution for both samples was analysed by histograms fitted with lognormal distribution function

for size analysis: $y = y_0 + \frac{A}{wx\sqrt{2\pi}}\, e^{\frac{-ln\frac{x^2}{xc}}{2w^2}}$. In this function, *xc* represents mean particle size diameter and *w* denotes the standard deviation [181].

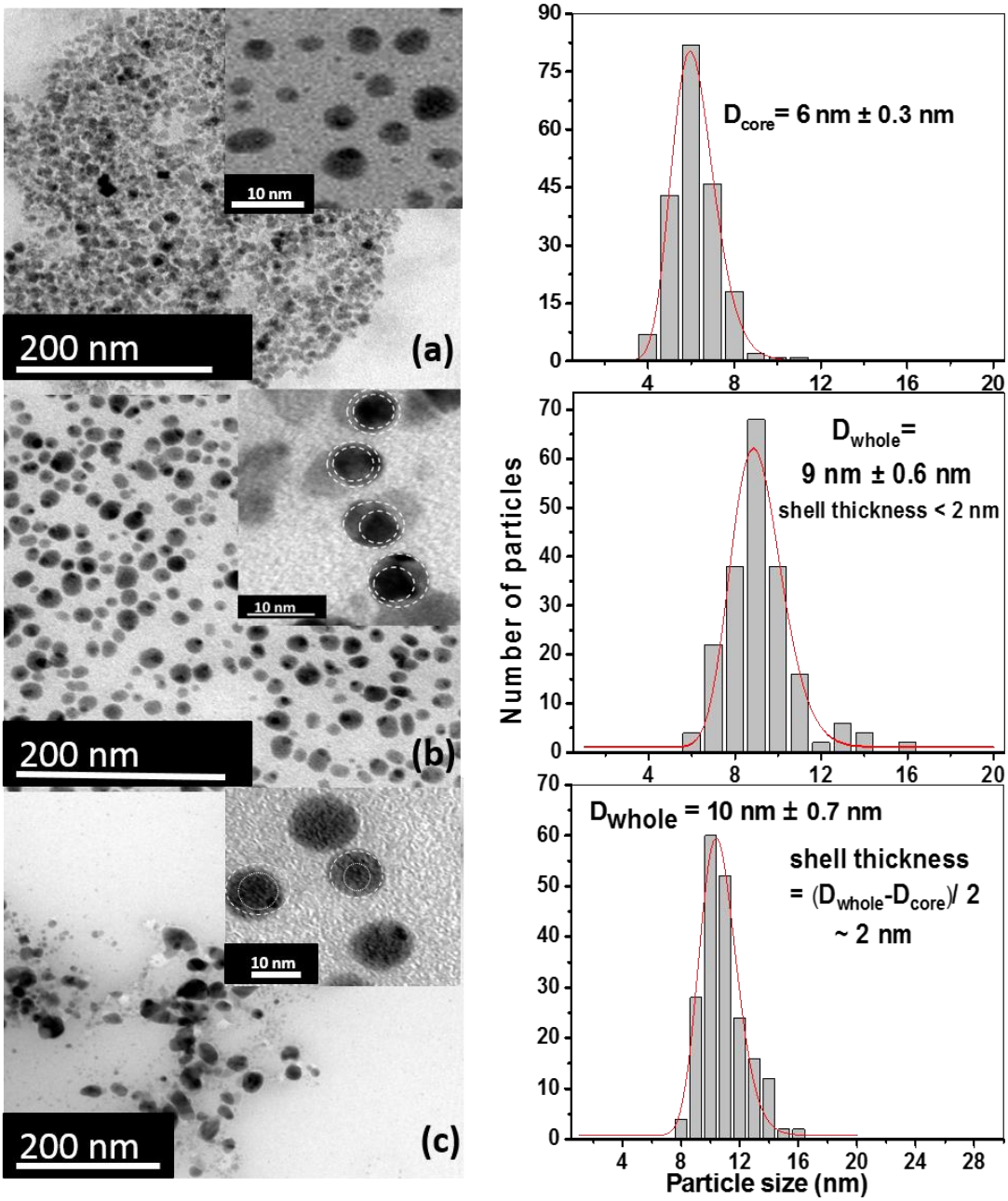

Figure 4.3 TEM images for (a) uncoated Fe_3O_4 nanoparticles; Ag@ Fe_3O_4 nanoparticles with shell thickness (b) < 2 nm and (c) ~2 nm (Inset- high-resolution TEM images for the nanoparticle system). The dotted and dashed lines highlight the contrast prevailing at core and shell boundaries, respectively. The adjacent histograms represent particle size distribution for respective nanoparticle system.

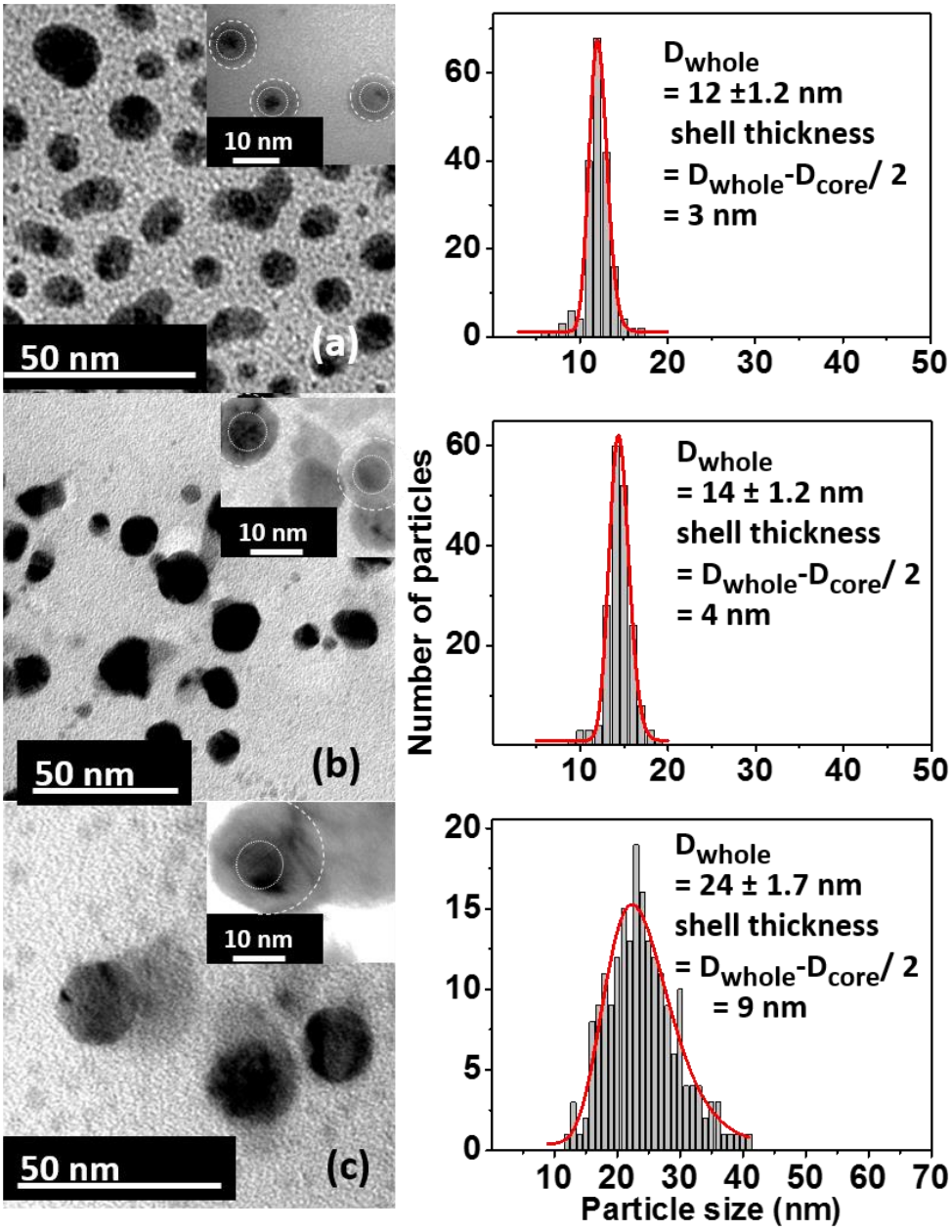

Figure 4.4 TEM images for (a) uncoated Fe_3O_4 nanoparticles; Ag@ Fe_3O_4 nanoparticles with shell thickness (b) ~3 nm, (c) ~4 nm and (d) ~9 nm (Inset- high-resolution TEM images for the nanoparticle system). The dotted and dashed lines highlight the contrast prevailing at core and shell boundaries, respectively. The adjacent histograms represent particle size distribution for respective nanoparticle system.

The mean particle size for uncoated magnetite (D_{core}) was found to be ~6 nm which is in good agreement with the values of crystallite size obtained using XRD data. The high resolution TEM images as shown in inset of Figure 4.3 & 4.4 clearly indicate contrast in a single distinct elements present in a single particle, i.e. magnetite and silver, confirms the formation of core-shell nanostructure. For the silver coated nanoparticles, the mean particle sizes (D_{whole}) are ~9 nm, ~10 nm, ~12 nm, ~14 nm and ~24 nm with small values of standard deviation from the mean values. This confirmed the formation of approximately thinner than 2 nm, ~2 nm, ~3 nm, ~4 nm and ~9 nm thick silver shells on the magnetite core of diameter ~6 nm. The lognormal fit for uncoated and coated nanoparticles gave small value of standard deviation confirming the narrow size distribution for ~6 nm core as well as thinner than 2 nm, ~2 nm, ~3 nm and ~4 nm thick silver coated nanoparticles. The narrow size distribution shows the superiority of the microemulsion synthesis method. The particles with ~9 nm shell shows a slightly larger standard deviation indicating relatively wider size distribution, but still narrow, in comparison with the nanoparticles obtained by other frequently used synthesis methods.

The quantitative analysis of the coated samples was carried out using EDX studies. The spot Energy Dispersive X- Ray Spectroscopy (EDX) measurement confirms increasing silver concentration in coated magnetic nanoparticles. A gradual increment in intensities of AgL spectra lines are in accordance with variable thickness of silver shell. The measured spectral lines of silver are more intense for 9 nm shell which reduces with decrease in shell thickness (Figure 4.5). An increase in atomic fraction of silver and decrease for iron is recorded for larger shell thickness. The values of atomic fraction for silver are found to be 25%, 30% and 74% for ~3 nm, ~4 nm and ~9 nm shell, respectively. The line EDX analysis in three samples represents the chemical homogeneity of the core-

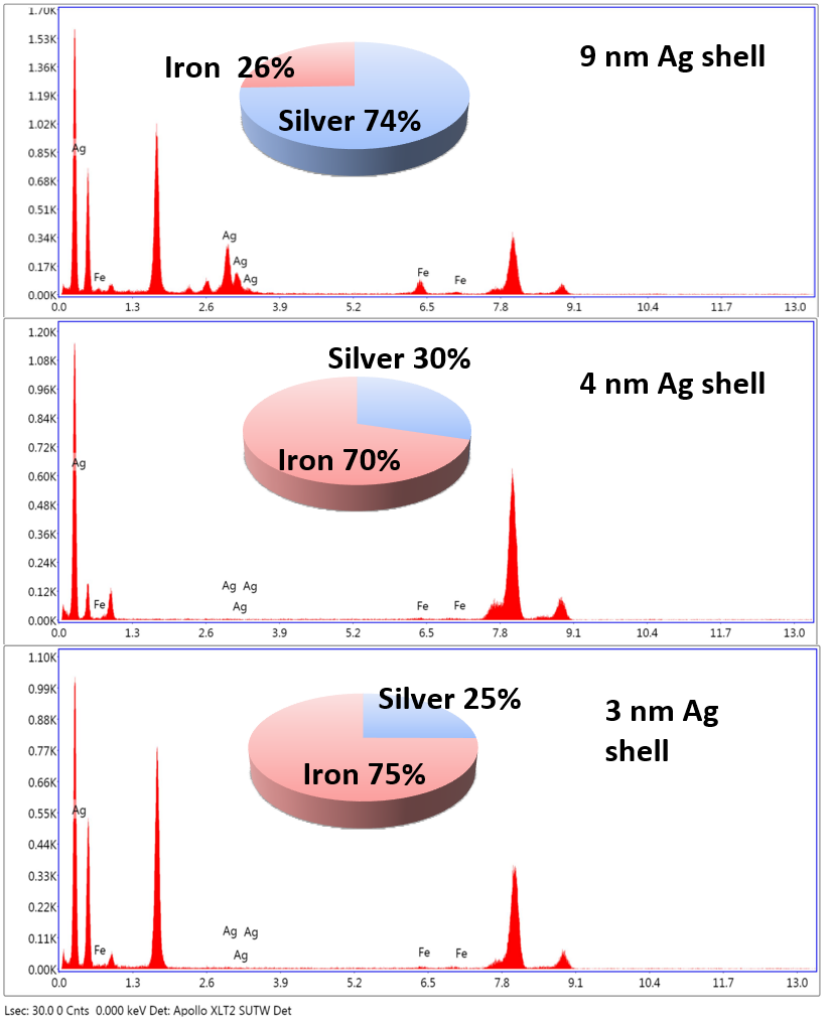

Figure 4.5 EDX spectrum obtained for silver coated magnetite nanoparticles with different shell thickness indicating increasing atomic percent of silver for thicker shells.

shell nanostructures. The theoretically calculated atomic fraction of silver for ~3 and ~4 nm thick shell coated particles are in good agreement with the values of the data obtained using EDXS revealing coating of a single magnetite nanoparticle with silver. On the other hand, comparing the theoretical value of atomic percent of silver in case of ~9 nm thick shell (which is obtained to be 98%) with EDXS data (~74 percent), we realize that amount of silver is less than estimated value, thus leading to a possibility of incorporating more than one Fe_3O_4 nanoparticle by silver shell. In order to get a much clear information

about the elemental composition and percentage of silver and iron in silver coated nanoparticles, three coated samples have been analysed using ICP-MS system. The data obtained through ICP-MS system is found to be in good agreement with the EDXS data. The concentration of silver is found to be 71.5, 32 and 27 percent for 9 nm, 4 nm and 3 nm thick silver shell coated magnetite nanoparticles, respectively. Figure 4.6 represents the pie chart depicting elemental composition obtained through ICP-MS.

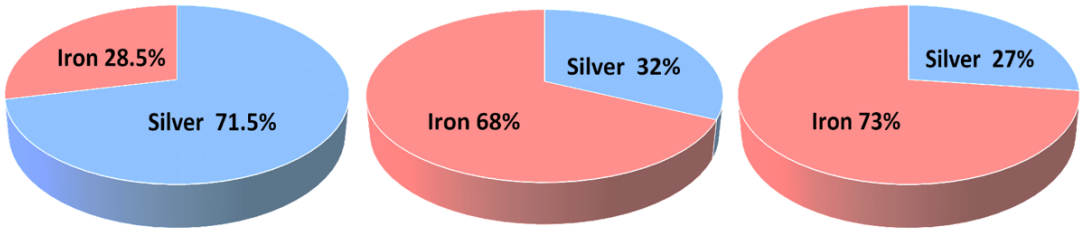

Figure 4.6 Pie chart showing elemental composition of 9 nm, 4 nm and 3 nm thick silver shell (in sequence) obtained using ICP-MS system.

The monodispersity of uncoated and coated nanoparticles are also evident from measurement of autocorrelation functions as well as hydrodynamic size obtained using DLS measurements (Figure 4.7). The autocorrelation function and hydrodynamic particle size is measured via dynamic light scattering method to explain and confirm the monodispersity of the uncoated as well as silver coated magnetite nanoparticles. The plot of autocorrelation function with decay time clearly indicates the monodispersity of samples. The hydrodynamic size is obtained as ~23 nm, ~42 nm, ~45 nm and ~47 nm for uncoated and ~3 nm, ~4 nm and ~9 nm thick silver shell coated magnetite nanoparticles. An obvious difference is visible in the particle sizes obtained from TEM and DLS method due to difference in chemical environments used in the techniques. The TEM measures the particle size in frozen or solid state whereas the DLS measures the behavior of particles in a solution based on their diffusion and hydration layer attached on the outermost part of nanoparticles.

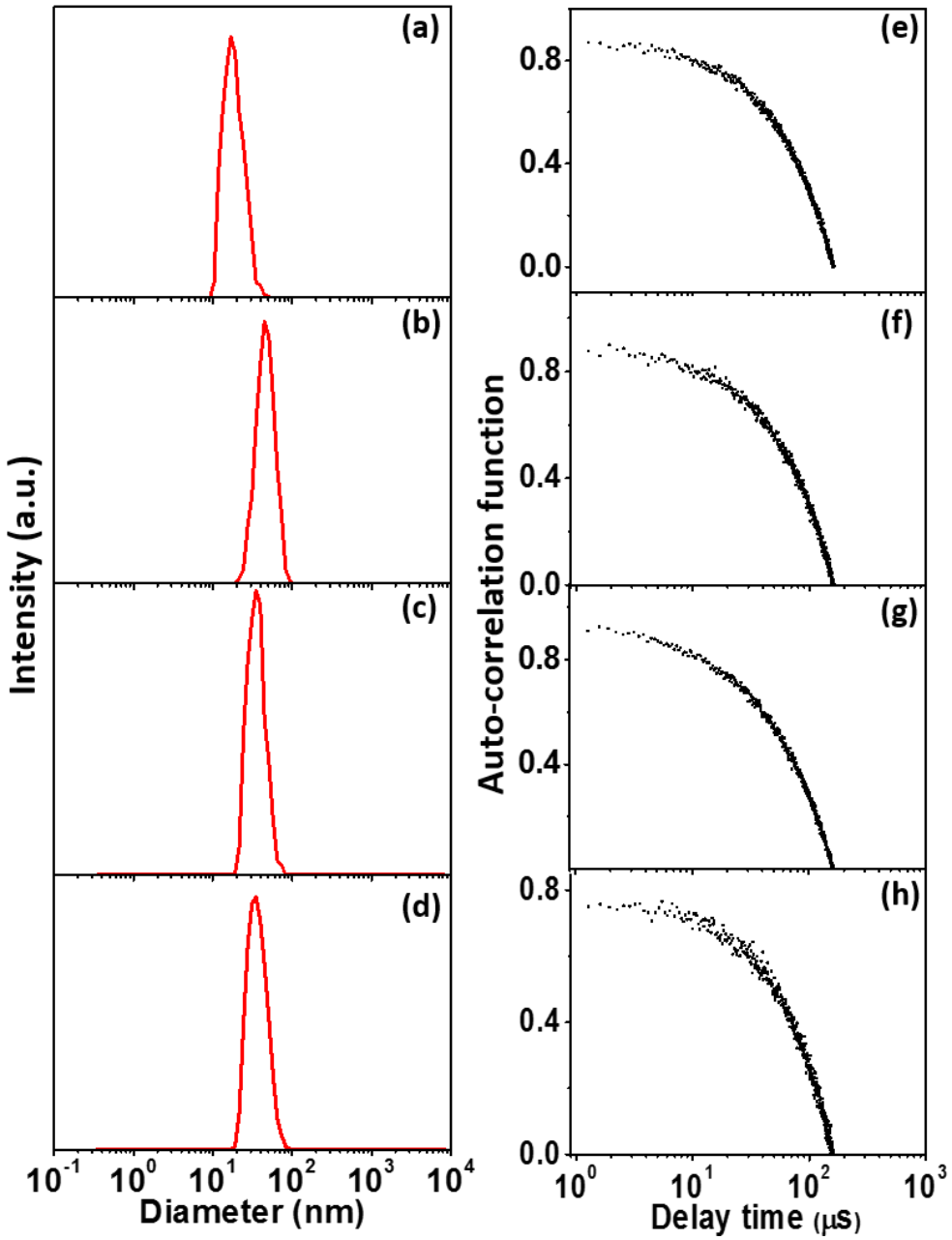

Figure 4.7 Hydrodynamic size and Correlation function of uncoated and coated samples measured using Dynamic Light Scattering method. Graphs a-d shows plot of intensity against particle diameter in nanometer range for uncoated, ~3 nm shell, ~4 nm shell and ~9 nm shell coated magnetite nanoparticles, respectively. Graphs e-h depicts autocorrelation function vs decay time for uncoated, ~3 nm shell, ~4 nm shell and ~9 nm silver shell coated Fe_3O_4 nanoparticles**.**

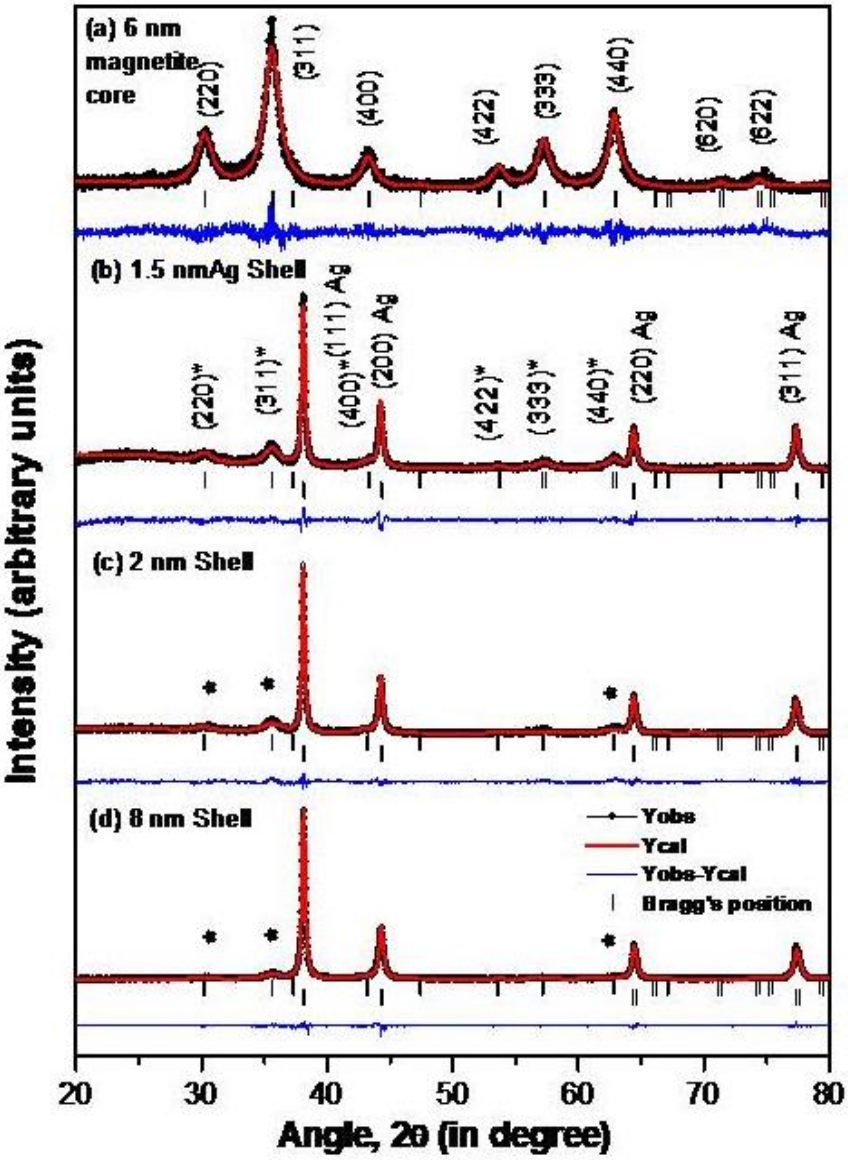

Figure 4.8 X-Ray diffraction patterns of (a) 6 nm uncoated magnetite; magnetite nanoparticles coated with varying thickness of silver shell (b) thinner than 2 nm (c) ~2 nm, and (d) ~8 nm. * indicates the reflections corresponding to magnetite phase in silver coated NPs.

Figure 4.7 demonstrates the measured auto-correlation function and hydrodynamic size for uncoated and coated nanoparticles. The XRD pattern for uncoated magnetite and silver coated magnetite nanoparticles with shell thickness thinner than 2 nm, ~2 nm and ~8 nm is shown in Figure 4.8 with their best fitted values using Le Bail refinement. The

patterns for coated nanoparticles were refined using Fe_3O_4 phase (space group $Fd\bar{3}m$, 227) and Ag phase ($Fm\bar{3}m$, 225). The unit cell parameter for uncoated iron oxide nanoparticle is observed to be 8.356 Å. On coating the same magnetite nanoparticle with silver shell thickness thinner than 2 nm, the unit cell length increases to 8.361 Å and further to 8.369 Å for 2 nm coating. This value of unit cell parameter becomes constant and almost no change incurs upon further increase of shell thickness onto the core. The refinement parameters such as conventional reliability factors, number of refined parameters and lattice parameters with error is shown in the Table 4.1.

This expansion of Fe_3O_4 unit cell parameter on coating with Ag metal can probably be

Table 4.1. Summary of reliability factors, numbers of parameters refined, and lattice parameters with error obtained for Le Bail refinement.

S. No.	Sample Name	R_p	R_{wp}	R_e	χ^2	Number of refined parameters	Lattice parameters with error
1	Magnetite NP (~6 nm)	20.9	28.3	22.5	1.586	6	8.356(2)
2	Ag coated Magnetite with ~ thinner than 2 nm shell	20.1	22.6	19.7	1.307	11	8.361(1)
3	Ag coated magnetite with ~2 nm shell	13.2	18.5	13.7	1.835	8	8.369(3)
4	Ag coated magnetite with ~8 nm shell	10.0	16.4	11.1	2.2	15	8.371(5)

associated with the interface effects between magnetite core and silver shell. The silver ion diffuses inside the core up to a certain thickness giving rise to a trilayer structure instead of a bilayer core- shell structure. The ionic radii of Ag^{+2} ion (0.94 Å) is larger

than that of Fe^{+2} and Fe^{+3} lower spin state ionic radii (Fe^{+2}= 0.61 Å and Fe^{+3}= 0.55 Å). There is a possibility that few silver ions diffuse in magnetite unit cell leading to the net expansion in unit cell parameter. This diffusion of sliver inside the core depends upon shell thickness for thin layers and becomes constant after a critical value of shell. This leads to formation of a diffused core layer in between the non- magnetic shell and magnetic core. As a consequence, a nanostructure with different component layers was obtained.

This observation has been further supported by magnetic measurements as well, which we have discussed in chapter 5 of the thesis.

4.3 Structural Characterization of Uncoated and Janus Shaped Silver-Magnetite Nanoparticles

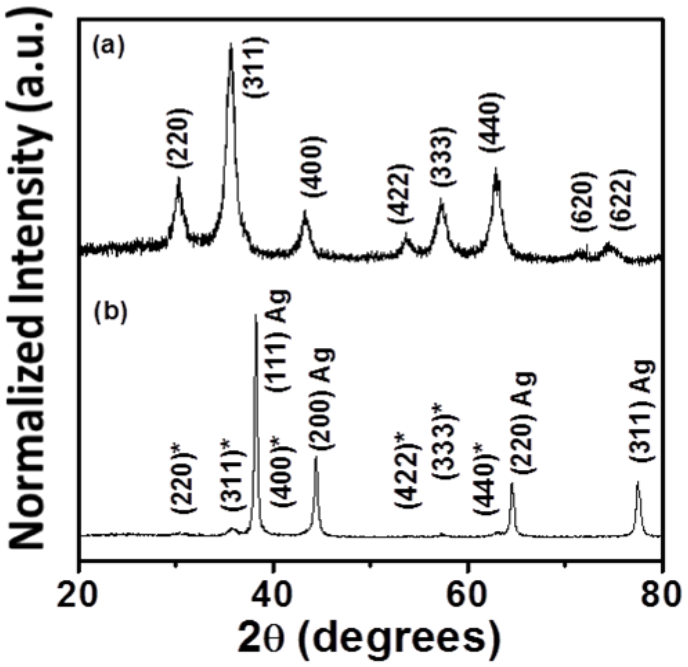

Figure 4.9 XRD pattern for (a) uncoated ~ 8 nm magnetite nanoparticles (b) Janus shaped silver-magnetite nanoparticles.

The X-ray diffraction (XRD) patterns for synthesized magnetite and silver-magnetite nanoparticles are shown in Figure 4.10. The analysis of XRD patterns in Figure 4.9 (a) indicates the formation of cubic spinel magnetite nanoparticles in pure phase (space group $Fd\bar{3}m$, 227). The XRD pattern for silver- magnetite nanoparticles (fig 4.9 (b)) shows the presence of silver with space group $Fm\bar{3}m$, 225 along with the characteristic peaks of magnetite. The larger Full Width at High Maximum (FWHM) values in XRD spectra indicates the formation of nanoparticles for both the samples. The crystallite size of pure phase magnetite nanoparticles is found to be 8 nm, calculated using Scherrer formula [162]. The X- ray diffraction pattern for silver-magnetite nanoparticles shows reflections corresponding to magnetite as well, with relatively very low intensity possibly due to higher electron density of silver.

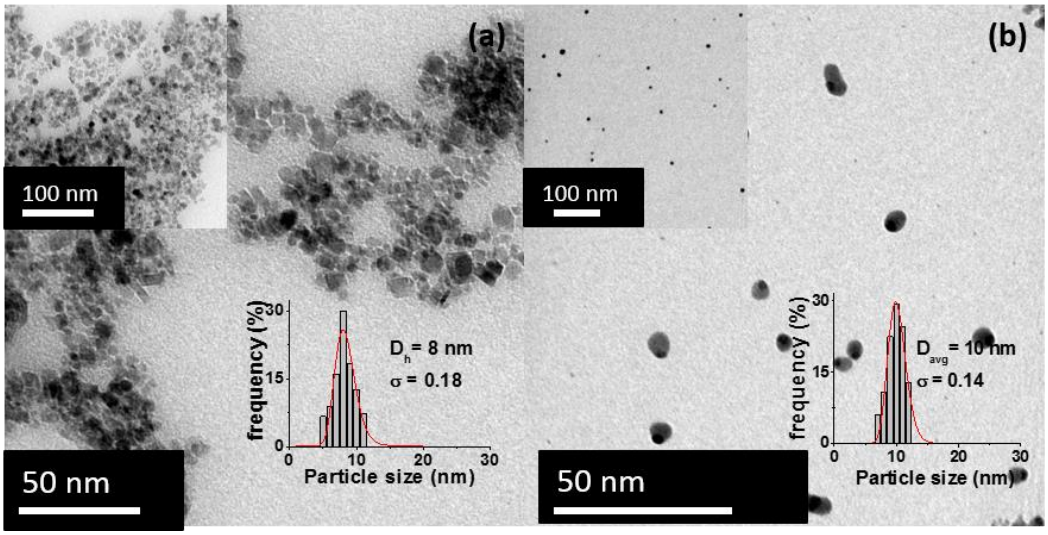

Figure. 4.10. Transmission Electron Micrographs of (a) bare magnetite nanoparticles; (b) Janus silver-magnetite nanoparticles. The inset in figures represents particle size distribution and their log normal fit with average particle size (D_{avg}) and standard deviation (σ). (Note- The size distribution histogram has been obtained using multiple TEM images.)

Figure 4.10 represents the Transmission Electron Microscopy (TEM) images and particle size distribution of the synthesized particles. The size distribution and average particle size of the uncoated and silver-magnetite nanoparticles were obtained by measuring size of nearly 200 particles using TEM micrographs. The mean particle size was found to be ~8 nm for pure phase magnetite nanoparticles. In case of silver-Fe_3O_4 Janus nanoparticles, the average particle size was found to be ~10 nm. The presence of contrast in TEM images for silver-magnetite Janus nanoparticles is observed due to varying electron penetration efficiency for different elements. The lognormal fit of histograms for magnetite and silver-magnetite nanoparticles gives a standard deviation of 0.18 and 0.14, respectively that emphasizes on narrow size distribution of synthesized nanoparticles.

The measurements of auto-correlation function versus delay time plot performed shows

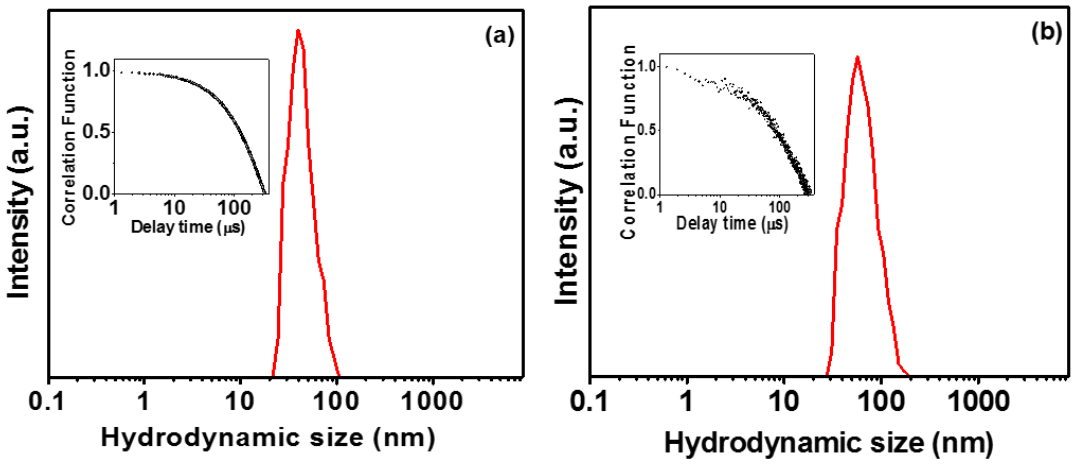

Figure 4.11 The particle size distribution chart obtained using dynamic light scattering method to calculate coated magnetite nanoparticles. The insets in figure show variation of correlation function with delay time. Hydrodynamic size (D_h) (a) uncoated ~8 nm magnetite nanoparticles; (b) silver coated magnetite nanoparticles. The insets in figure show variation of correlation function with delay time.

a single which confirms the presence of monodispersed particles in the solution for magnetite as well as silver-magnetite Janus samples (inset of Figure 4.11). The hydrodynamic size of the magnetite and silver-magnetite nanoparticles is found to be 71 and 131 nm which is higher than the particle sizes obtained through TEM images (Figure 4.11).

The synthesized magnetite and silver-magnetite nanoparticles were found to be highly stable using zeta potential measurement. It is a measure of electric potential between the dispersed and medium charged entities at the surface of a nanoparticle. The zeta potential values lying in the range between 0 to ±5 mV and ±10 to ±30 mV indicates rapid coagulation and nascent instability of samples, respectively. The zeta potential values for stable systems are categorised in three ranges ±30 to ±40 mV, ±40 to ±60 mV and above ± 60 mV. These ranges correspond to moderate stability, good stability and excellent stability of nanomaterials, respectively. The zeta potential values obtained for magnetite and silver-magnetite nanoparticles are obtained to be −67.39 mV and −74.6 mV, respectively. These values suggest the strongly electron rich nature of the nanoparticles. It can be inferred from the experimental values that synthesized samples, magnetite and silver-magnetite nanoparticles, are very highly stable. The integration of magnetite nanoparticles with silver increases the zeta potential resulting in enhancement of electrostatic repulsion among nanoparticles that further enhances its stability.

4.4 Conclusion

The magnetite, silver coated magnetite core-shell nanostructures and Janus shaped silver-magnetite nanoparticles have been obtained and characterized for their phase purity, size and shape. The monodispersity of the samples have been confirmed through DLS measurements. From structural analysis through Le Bail refinement of XRD data, we report that the core-shell nanostructure is not exactly bilayer core- shell but a structure

with disordered magnetic shell in between magnetite core and outermost silver layer. Further, magnetic studies discussed in next chapter agree with our assumption and confirms the presence of intermediate spin disordered layer.